Properties of galaxy haloes in clusters and voids

V. Antonuccio-Delogu,[1]★† U. Becciani,[1] E. van Kampen,[2] A. Pagliaro,[3] A. B. Romeo,[4] S. Colafrancesco,[5] A. Germaná[1] and M. Gambera[6]

[1]*Osservatorio Astrofisico di Catania, Cittá Universitaria, Via Santa Sofia 78, 95123 Catania, Italy*
[2]*Institute of Astronomy, University of Edinburgh, Blackford Hill, Edinburgh EH9 3HJ*
[3]*SRON, 3584 CA Utrecht, the Netherlands*
[4]*Department of Astronomy and Astrophysics, Centre for Astrophysics and Space Science, Chalmers University of Technology, SE-43992 Onsala, Sweden*
[5]*Osservatorio Astronomico di Roma, Monteporzio Catone, Italy*
[6]*Liceo Scientifico Statale 'E. Majorana', Scordia, Italy*

ABSTRACT

We use the results of a high-resolution *N*-body simulation to investigate the role of the environment on the formation and evolution of galaxy-sized haloes. Starting from a set of constrained initial conditions, we have produced a final configuration hosting a double cluster in one octant and a large void extending over two octants of the simulation box. In this paper we concentrate on gravitationally bound galaxy-sized haloes extracted from these two regions and from a third region hosting a single, relaxed cluster without substructure. Exploiting the high mass resolution of our simulation ($m_{body} = 2.1 \times 10^9 \, h^{-1} \, M_\odot$), we construct halo samples probing more than two decades in mass, starting from a rather small mass threshold: $5 \times 10^{10} \, h^{-1} \, M_\odot \leq M$. We present results for two statistics: the relationship between one-dimensional velocity dispersion σ_v and mass M_0 and the probability distribution of the spin parameter $P(\lambda)$, and for three different group finders. The σ_v–M_0 relationship is well reproduced by the truncated isothermal sphere (TIS) model introduced by Shapiro et al., although the slope is different from the original prediction. A series of σ_v–M_0 relationships for different values of the anisotropy parameter β, obtained using the theoretical predictions by Łokas & Mamon for Navarro et al. density profiles, are found to be only marginally consistent with the data. Using some properties of the equilibrium TIS models, we construct subsamples of *fiducial* equilibrium TIS haloes from each of the three subregions, and we study their properties. For these haloes, we do find an environmental dependence of their properties, in particular of the spin parameter distribution $P(\lambda)$. We study the TIS model in more detail, and we find new relationships between the truncation radius and other structural parameters. No gravitationally bound halo is found having a radius larger than the critical value for gravithermal instability for TIS haloes ($r_t \geq 34.2 r_0$, where r_0 is the core radius of the TIS solution). We do, however, find a dependence of this relationship on the environment, like for the $P(\lambda)$ statistics. These facts hint at a possible role of tidal fields in determining the statistical properties of haloes.

Key words: methods: *N*-body simulations – galaxies: formation – galaxies: haloes – large-scale structure of Universe.

1 INTRODUCTION

One of the distinguishing features of any scenario for the formation of the large-scale structure of the Universe within the cold dark matter (CDM) cosmological model is represented by the

hierarchical clustering paradigm for the assembly of gravitationally bound structures (White 1996, 1997). In its simplest form, the idea of hierarchical clustering implies that the growth of haloes proceeds by accretion of smaller units from the surrounding environment, either by infall (Gunn & Gott 1972) or by a series of 'merging' events (White & Rees 1978), whereby the subunits are accreted in a discontinuous way, or (more likely) by a combination of the two. In the first case the typical halo profiles evolve

---

adiabatically, while in the merging scenario each merging 'event' will induce some transients in the characteristic properties which in turn will induce some evolution in the typical profiles, after the subunits have been accreted and destroyed. In either case, one expects that relaxation processes should drive the evolution towards a quasi-equilibrium state on a dynamical time-scale, a state characterized by relationships among global quantities related to the halo, like its mass, density, velocity dispersion σ_v, and possibly others. Recently considerable attention has been devoted to the study of one of these relationships: the radial dependence of the (spherically averaged) density, also known as the density profile. Unfortunately the density profile is a very difficult tool to use when trying to characterize the statistical properties of halo populations, because the predictions of different models of halo formation differ only in the behaviour in the central parts, where the statistics are typically poor. Less attention has been paid to another global quantity, namely the velocity dispersion, and to its relationship with other global quantities, like the mass. The velocity dispersion enters the second-order Jeans equation, while the density profile is described by the zeroth-order Jeans equation (Binney & Tremaine 1987). For this reason it contains different physical information from the density profile. Recently Bryan & Norman (1998) have looked at the σ_v–M_0 relationship for clusters, and they find a good agreement with the standard, singular isothermal sphere model as far as the slope of the relationship is concerned. Also Knebe & Müller (1999) looked at this relationship, using a different code. Halo equilibrium models make predictions about the σ_v–M_0 relationship, but these are difficult to compare with observations, because some of the involved quantities (e.g. the velocity dispersion itself) are not directly deducible from observations. They can, however, be studied with *N*-body simulations, and one of the purposes of this paper will be to show that the σ_v–M_0 relationship can be used to discriminate among different halo equilibrium models.

A second problem that we will study concerns the dependence of halo properties on the environment within which they form. In both the hierarchical clustering scenarios mentioned above one could imagine that the properties of the haloes do depend on the environment. For instance, the dynamics of the infall process could be affected by the average overdensity of the environment within which the halo grows (Gunn 1977), or by its shear (Buchert, Kerscher & Sicka 1999; Takada & Futamase 1999). Also typical quantities related to the merging, like the frequency of merging events, could intuitively be affected by the average density of the environment, at least for galaxy-sized haloes forming within clusters. High-resolution *N*-body simulations (e.g. Moore et al. 1999) show that most of the galaxies lying in the central (i.e. virialized) parts of clusters do not easily reach a velocity larger than the escape velocity, so they are bound to the cluster for the largest part of their evolutionary history, and consequently form in an overdense environment. It would then be interesting to try to understand whether there are systematic differences between haloes forming in clusters and in voids.

Some of these issues have been recently discussed in the literature. Lemson & Kauffmann (1999) have analysed the dependence of various statistical properties, including the spin probability distribution, on the environment, and found no evidence for any dependence apart from the extent of the mass spectrum. They divide their haloes into groups according to the overdensity of the environment within which they are found, and show that the scatter diagrams between different quantities are indistinguishable among the different groups. In the present study,

we follow a different strategy. We study a simulation obtained from a constrained set of initial conditions, in order to get a few clusters (and, in particular, a double cluster) and a large void within the same simulation box. We then extract our haloes from three spatially disjoint regions: one containing a double cluster, a second one containing a single cluster, and a third one containing the void. This is in some sense complementary to the procedure which Lemson & Kauffmann seem to have followed, because our haloes are grouped according to the spatial distribution, rather than according to the overdensity, so they are grouped according to the *environment* within which they form.

Very recently Gardner (2000) presented a study of the spin probability distribution for six different cosmological models and environments. He finds a difference between the distributions of haloes resulting from recent mergers and haloes that did not experience mergers, almost independently of the environment within which they form. This could have significant consequences for the construction of merger histories, and, ultimately for the semi-analytical modelling of galaxies. Similar results have been recently obtained by Vitvitska et al. (2001).

The plan of the paper is as follows. In Section 2 we describe the numerical setup of the simulations and the algorithm adopted to identify haloes. In Section 3 we describe the halo equilibrium models with which we compare the results of our simulation, and in Section 4 we show the results of this comparison and discuss their physical interpretation. Finally, in the conclusions we summarize our results and suggest some directions for future studies.

In the following we will always assume a $\Omega = 1$ standard CDM model, with a Hubble constant $H_0 = 100\,h\,\mathrm{km\,s^{-1}\,Mpc^{-1}}$, and $h = 0.5$. All lengths, unless explicitly stated, are assumed to be comoving.

2 SIMULATIONS

The simulation from which the data have been extracted has been performed using FLY (Becciani et al. 1997, 1998), a parallel, collisionless treecode optimized for shared memory and/or clustered computing systems. FLY deals with periodic boundary conditions using a standard Ewald summation technique (Hernquist, Bouchet & Suto 1991). The algorithm adopted is the octal-tree algorithm of Barnes and Hut (Barnes & Hut 1986), with some modifications ('grouping' of cells belonging to the lists of nearby particles: Barnes 1987) during the phase of tree walking. These changes have a negligible impact on the overall numerical accuracy, as shown elsewhere (Becciani, Antonuccio-Delogu & Gambera 2000), but they have a strong positive impact on parallel performance and scaling.

We have performed two simulations starting from the same initial conditions. In both cases the underlying cosmological model is a standard CDM (SCDM) model, with $\Omega_0 = 1$, $\sigma_8 = 0.9$. The main reason for this choice lies in the fact that the specific prediction for the σ_v–M_0 statistics that we consider in the next sections was done for this particular cosmological model. We plan to extend our work to other cosmological models in future.

Each simulation used 256^3 particles, and the box size was $50\,h^{-1}\,\mathrm{Mpc}$, so that the mass of each particle is $m_{\mathrm{part}} = 2.07 \times 10^9\,h^{-1}\,\mathrm{M_\odot}$. The simulations were designed to study the evolution of a Coma-like cluster, and for this purpose constrained initial conditions were prepared, changing only the softening length, which was fixed to $\epsilon = 10$ and $5\,h^{-1}\,\mathrm{kpc}$, respectively. As far as the results presented in this paper are concerned, there are no
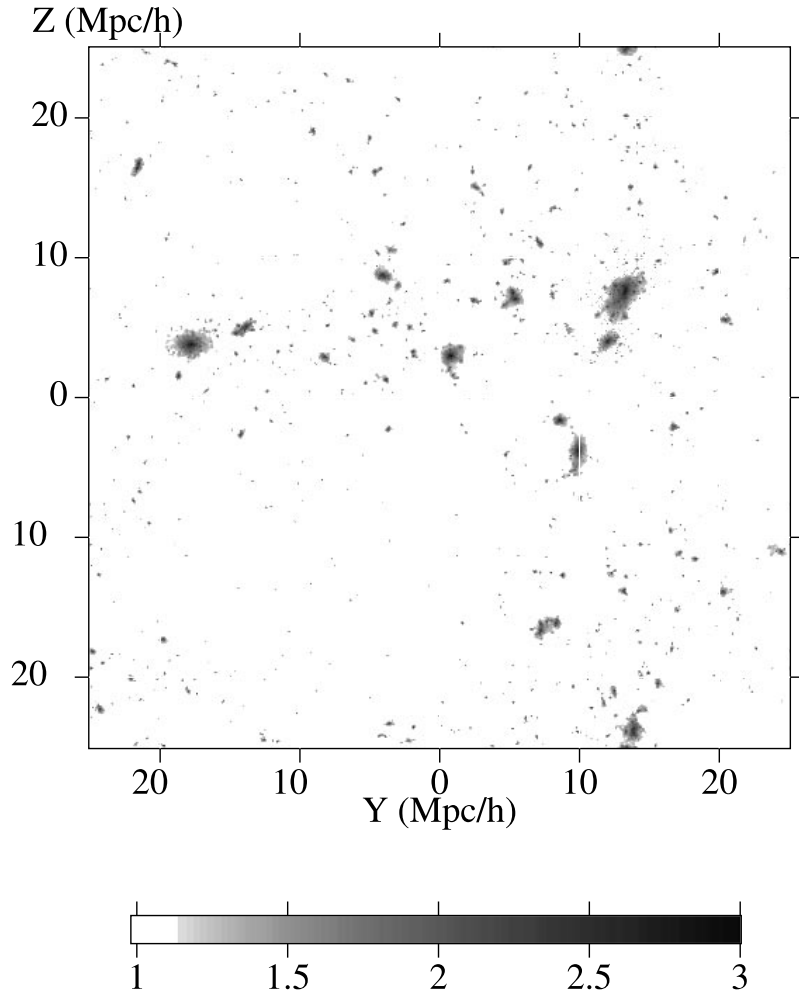
Figure 1. Snapshot of the simulation box at the end of the simulation. The scale of grey corresponds to density in logarithmic units. The large void is clearly seen in projection extending over the lower left octant.

Table 1. Properties of the analysed regions.

Region	x	y	z	L	Number of haloes
DOUBLE	15	12.5	7.5	10	827
SINGLE	12	−18	4	10	786
VOID	−10	−10.	−10.	20	609

All lengths are in h^{-1} Mpc. From left to right, columns are as follows: label of the region, x, y, and z coordinates of its centre, size of the region, total number of haloes found.

differences among these two simulations, so for the rest of this paper we will concentrate only on the simulation with the largest softening length, which we designate in the following as 16ML_1.

Constrained initial conditions were prepared using the implementation of the constrained random field algorithm of Hoffman & Ribak (1991) by van de Weygaert & Bertschinger (1996). We took the same initial conditions as adopted in one of the simulations from the catalogue of van Kampen & Katgert (1997). More specifically, we constrained the initial conditions to have a peak at the centre of the simulation box, with height 3.04σ, Gaussian smoothed at a scale of $6\,h^{-1}$ Mpc, and a -2σ void centred at $(15, 0, -10)$. The final configuration is shown in Fig. 1. In order to study the environmental dependence of the properties of galaxy-sized halo populations, we selected three regions within the

computational box, which we call DOUBLE, SINGLE and VOID. All the three are cubical with centres and sizes as specified in Table 1. The DOUBLE region hosts a double cluster, with two large parts in the act of merging by the end of the simulation (see Fig. 2). The SINGLE region hosts a more relaxed cluster without any apparent substructure. Finally, we have included in the analysis a significantly underdense region, the VOID, which is more extended than the former two, so as to contain enough haloes to allow reasonable statistics.

2.1 Finding haloes

Various methods have been devised to extract haloes from the outputs of *N*-body simulations. Some of these methods make use only of particle positions, like the standard friends-of-friends (hereafter FOF) and the various versions of the adaptive FOF, while others take into account also particle velocities (e.g. SKID: Governato et al. 1997) and/or environmental properties like local densities (like HOP: Eisenstein & Hut 1998). Most of the results we will present later have been obtained using SKID because it selects *gravitationally bound* groups of particles. In short, SKID first builds catalogues of groups using a standard FOF algorithm, selecting only particles lying within regions with density larger than a critical value δ_{crit}. It then computes the escape velocity of each particle and discards those particles having an rms velocity
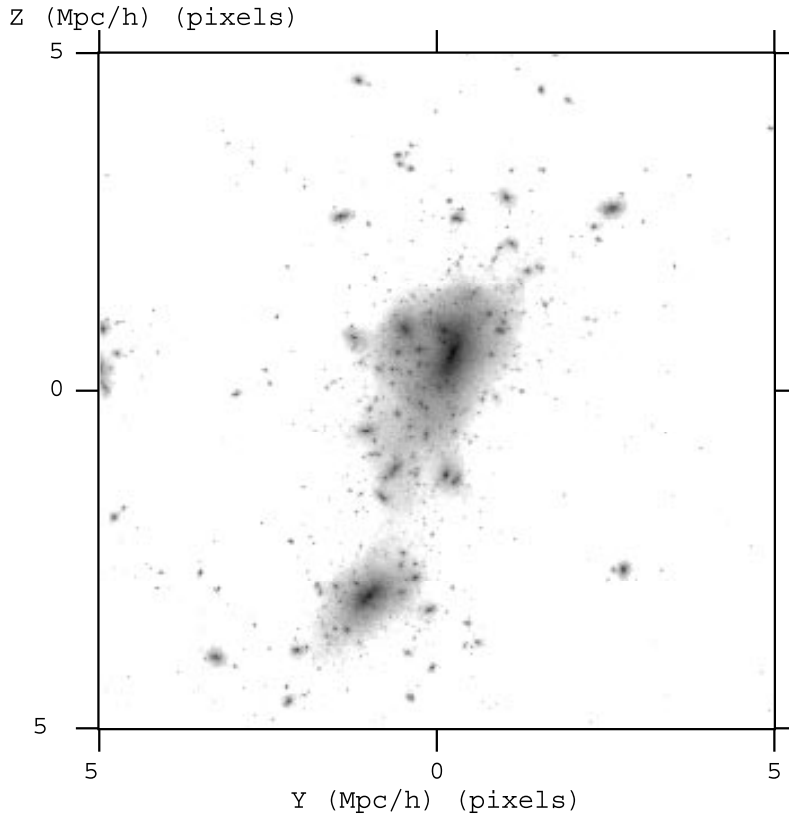
Figure 2. The region of the DOUBLE cluster.

larger than the escape velocity. This 'pruning' procedure should then leave only those particles that are actually bound to the group, discarding those 'background' particles that find themselves by accident at a given time within it. The initial linking length of the FOF phase determines the approximate size of the groups that we are considering. We assumed a linking length of $100\,h^{-1}\,$kpc, corresponding to the typical size of a galaxy-sized object at the present epoch. The softening length for the calculation of the gravitational potential was assumed to be the same as in the simulation, and the critical density δ_{crit} was set equal to $178/(1+z)$, the value for non-linear collapse in the Gunn & Gott collapse model, so that only particles from genuinely non-linearly collapsed shells should be included.

Following a suggestion by the anonymous referee, we have also adopted two more halo finders to check the robustness of the results: an adaptive FOF method devised by van Kampen & Katgert (1997) and a modified version of SKID which should avoid the problems posed by the original version. This particular adaptive FOF halo finder selects only those haloes that are virialized, by specifically testing for virialization. Concerning the second method, we have modified SKID only in that part which generates the input group list which is subsequently 'pruned' of the non-gravitationally bound particles: in place of a standard FOF (as in the original version of SKID) we have adopted HOP (Eisenstein & Hut 1998) as input group finder. As we will see later, some of the relationships that we find do depend on the group finder adopted, but those relationships holding for the equilibrium truncated isothermal sphere haloes are not affected by this. All the results that we present in the following are for the final redshift of the simulation, $z = 0.0047$, unless otherwise stated.

3   HALO EQUILIBRIUM MODELS

The internal properties of haloes formed by gravitational collapse can be described by looking at correlations among different physical quantities. The density profile has often been used to study the properties of relaxed, virialized haloes, particularly since the finding by Navarro, Frenk & White (1996) that this profile has a *universal* character when expressed in dimensionless units. However, the density profile can be reliably determined only for haloes having enough particles in each shell to minimize the statistical fluctuations. For instance, Navarro, Frenk & White (1997) considered only eight haloes extracted from a low-resolution simulation and re-simulated with a higher mass resolution.

Typical *N*-body simulations on cluster scales tend to produce a large amount of haloes, the density profile of which cannot be reliably determined, because each of them contains on average fewer than 10^5 particles. For this reason we have chosen to study relationships involving *global* halo properties. This choice is not free from potential problems: systematic biases can be introduced by the particular group finder adopted. Consider for instance SKID, which works by stripping out gravitationally unbound particles from haloes built using FOF: the group catalogues so produced tend to be more biased towards less massive haloes than catalogues produced using FOF. We have therefore decided to adopt three different group finders, in order to be able to understand the role of these systematic factors. We have also considered two different statistics to characterize the properties of dark matter haloes, and particularly their equilibrium properties at the end of the simulation: the internal one-dimensional velocity dispersion–mass relationship ($\sigma_v - M_0$) and the spin probability distribution

$P(\lambda)$. Theoretical predictions concerning both of them are available in the literature. In particular, we will compare the results from our N-body simulations with four models: the standard uniform isothermal sphere (SUS) model (see e.g. Padmanabhan 1993, ch. 8, for a detailed treatment), the truncated isothermal sphere (TIS) model recently introduced by Shapiro, Iliev & Raga (1999), the 'peak-patch' (PP) Monte Carlo model by (Bond & Myers (1996a), and a model derived from the Navarro et al. (1996, 1997) (hereafter NFW) density profiles. The first two models predict a σ_v–M_0 relationship given by

$$\sigma_v = c_f M_{12}^{1/3} (1 + z_{\text{coll}})^{1/2} \, h^{1/3} \, \text{km s}^{-1}, \tag{1}$$

where the subscript $f \equiv$ SUS or TIS, while for the PP model the relation is given in Bond & Myers (1996b):

$$\sigma_v = c_{\text{PP}} M_{12}^{0.29} (1 + z_{\text{coll}})^{1/2} \, h^{1/3} \, \text{km s}^{-1}. \tag{2}$$

In the equations above M_{12} is the mass in units of $10^{12} \, \text{M}_\odot$ and z_{coll} is the collapse redshift. The coefficients for these cases are given by

$$c_{\text{SUS,TIS,PP}} = (71.286, \quad 104.69, \quad 117.60) \tag{3}$$

respectively. We restrict our attention to these four models because the physical ingredients that enter in their formulation are very different, and encompass a sufficiently wide range among all the possible non-linear collapse and virialization mechanisms. This wide choice reflects our generally poor level of understanding of the non-linear physics of gravitational collapse, and of its dependence on the local environment and on other properties like the merging history of the substructures.

The SUS model is based on the spherical non-linear collapse model (Gunn & Gott 1972). In this model the collapse towards a singularity of a spherically symmetric shell of matter in a cosmological background is halted when its radius reaches a value of half the maximum expansion radius. The velocity dispersion is then fixed by imposing the condition of energy conservation, which must hold in the case of collisionless dark matter such as that envisaged here. The TIS model also considers the highly idealized case of a spherically symmetric configuration, but assumes that the final, relaxed system is described by an isothermal, isotropic distribution function and that the density profile is truncated at a finite radius. Shapiro et al. (1999) have shown that this configuration could arise from a top-hat collapse of an isolated spherical density perturbation if, as shown by Bertschinger (1985), the dimensionless region of shell crossing almost coincides with the region bounded by the outer shock in an ideal gas accretion collapse with the same mass (in an $\Omega = 1$ CDM model). The truncation radius is then assumed to coincide with the region of shell crossing, and this allows them to specify the model completely.

The PP model introduced by Bond & Myers (1996a) is more general than the SUS model, in that it includes a more realistic collapse model where deviations from spherical symmetry are taken into account. The density perturbation is approximated as an axisymmetric homogeneous spheroid. Coupling between the deformation tensor and the external and internal torques is consistently taken into account up to a few first orders, and Monte Carlo realizations are used to build up catalogues of haloes. These have been compared with the N-body simulations of Couchman (1991) in order to normalize the statistics properly. Note that equation (2) is a best-fitting relationship and holds for a range of halo mass ($2.5 \times 10^{14} \leq M_{\text{h}} \leq 5 \times 10^{15} \, \text{M}_\odot$) much larger than that considered here. None the less, we include it in our comparison

because the physical model on which it is based is significantly different from the other models we consider.

Finally, we have considered a model for the σ_v–M_0 statistics consistent with the NFW density profile, which was recently derived by Łokas & Mamon (2001) by solving the second-order Jeans equation:

$$\frac{1}{\rho} \frac{\text{d}}{\text{d}r} (\rho \sigma_r^2) + 2\beta \frac{\sigma_r^2}{r} = -\frac{\text{d}\Phi}{\text{d}r}, \tag{4}$$

where $\beta = 1 - \sigma_\theta^2(r)/\sigma_r^2(r)$ quantifies the anisotropy of the velocity dispersion. For an NFW density profile we have

$$\rho_{\text{NFW}}(r) \equiv \rho_{\text{NFW}}(s) = \frac{\rho_c^0 c^2 g(c)}{3} \frac{1}{s(1 + cs)^2}, \tag{5}$$

$$\Phi_{\text{NFW}}(s) = -\frac{GM_{\text{VIR}}}{r_{\text{VIR}}} g(c) \frac{\ln(1 + cs)}{s}, \tag{6}$$

where we have defined r_{VIR} and M_{VIR} as the virialization radius and mass, respectively, $s = r/r_{\text{VIR}}$, $c = c(M, z)$ is the concentration parameter and $g(c) = 1/[\ln(1 + c) - c/(1 + c]$. Equation 4 can be solved by quadrature, and the solution finite in the limit $r \to \infty$ is

$$\frac{\sigma_r^2}{V_v^2} (s, \beta = \text{constant}) = g(c)(1 + cs)^2 s^{1-2\beta}$$

$$\times \int_s^\infty \left[\frac{s^{2\beta-3} \ln(1 + cs)}{(1 + cs)^2} - \frac{cs^{2\beta-2}}{(1 + cs)^3} \right] \text{d}s. \tag{7}$$

Note that we have always chosen as critical threshold for our group finders the virialization overdensity ($\delta \geq \delta_{\text{crit}} = 178$), so the quantities r_{VIR} and M_{VIR} are the actual radius and mass found by the group finders for each halo.

In order to make use of equation (7) we have yet to specify the dependence of the concentration parameter on the mass at the final redshift: $c = c(M, z = 0)$. We adopt the relationship provided by Bullock et al. (2001), by running their code CVIR for the relevant cosmological model. In the mass range in which we are interested ($5 \times 10^{10} \leq M/\text{M}_\odot \leq 5 \times 10^{13}$) we find a power-law fit: $c(M, z = 0) = 472.063 \times M^{-0.127 \pm 0.01}$. Finally, in order to make a proper comparison with the quantity computed by the group finder, we evaluate the mass-averaged velocity dispersion:

$$\sigma_v^2 = \frac{4\pi \int_0^1 \sigma_{v,\text{NFW}}^2(s) \rho(s) s^2 \, \text{d}s}{M(1)}, \tag{8}$$

where we have defined

$$\sigma_{v,\text{NFW}}^2 = \sigma_r^2 + \sigma_\theta^2 = (2 - \beta)\sigma_r^2$$

and

$$M(1) = 4\pi \int_0^1 \rho(s) s^2 \, \text{d}s.$$

4 STATISTICAL PROPERTIES

4.1 The σ_v–M_0 relation

In Fig. 3 we show plots of the final σ_v–M_0 relationship for galaxy-sized haloes in the DOUBLE, SINGLE and VOID regions, respectively, obtained using SKID. The most striking difference is probably the different character of haloes in the VOID region when compared with the clustered regions. Haloes in VOID have a much smaller dispersion around the mean than haloes in the clustered
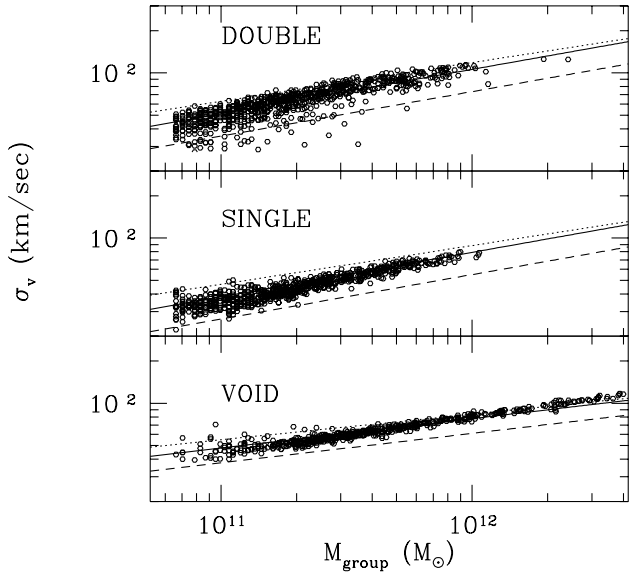
Figure 3. One-dimensional velocity dispersion versus mass for haloes extracted from the three regions. The three fitting curves correspond to the three cases considered in the text: truncated isothermal sphere (continuous line), Bond & Myers (1996b) (dotted line), and standard uniform sphere (dashed line). Note the larger mass extent for haloes in the VOID. In all the cases, the slope is larger than predicted by models, although within clusters the statistical uncertainty is large.
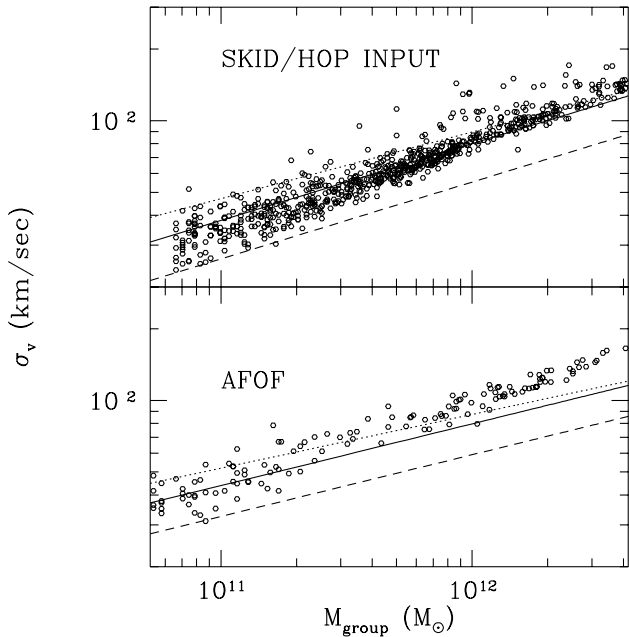
Figure 4. One-dimensional velocity dispersion versus mass for the DOUBLE cluster region; haloes selected using the adaptive FOF and modified SKID with HOP input group finders. The same parameters as adopted for SKID in Fig. 3 are adopted. The best-fitting power law for the plot in the upper figure has a slope $\alpha = 0.039 \pm 0.05$. The symbols for the fitting lines are as in Fig. 3.

regions, and the distribution is almost symmetric with respect to the best-fitting approximation. Haloes in the DOUBLE region have a larger dispersion and they do show an asymmetry in the distribution around the best-fitting solution, i.e. an excess of low-mass haloes at low σ_v. The latter point is useful to understand the potential systematic effects introduced by a particular group finder.
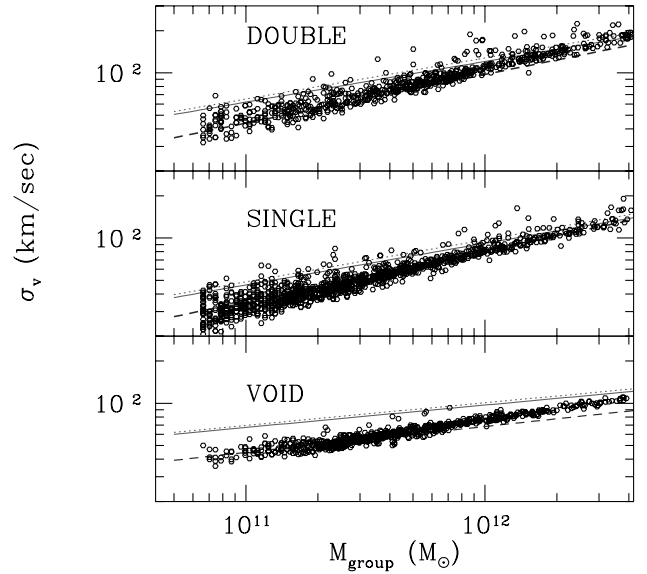
Figure 5. The σ_v–M_0 relationship for three models based on the NFW density profile. Continuous line: $\beta = 0$, slope of the r_{VIR}–M_{VIR} relation given by $\alpha = \alpha_{mean}$. Dotted line: $\beta = 0.5$, $\alpha = \alpha_{mean}$. Dashed line: $\beta = 0$, $\alpha = \alpha_{mean} - \Delta\alpha$ (i.e. the 1σ limit).

In Fig. 4 we show the σ_v–M_0 relationship for the DOUBLE region obtained by using the two other group finders mentioned above. As is evident, the excess of low-mass haloes is only an artefact introduced by SKID, which makes use of an FOF algorithm to build up an input list of groups. The main results of the next sections, however, do not depend on the particular group finder adopted, because we will select subsamples of haloes which can be regarded as *equilibrium TIS* haloes, and for them the slope of the σ_v–M_0 relationship is independent of the particular group finder initially adopted.

A more important difference is evident from a comparison between clustered and void regions. Haloes in VOID have a larger mass extent (a property already noted by Lemson & Kauffmann 1999) and also the slope of the σ_v–M_0 relation seems to be larger than for the other two cases.

In Fig. 5 we show a comparison with some theoretical predictions for NFW density profiles. In order to apply equations (6) and (7) we have still to specify a relationship between the virial radius and the corresponding mass, which enters into equation (6). In Fig. 6 we can see that there is a clear relationship between the truncation radius ζ_t and the mass, but we have to find a relationship between r_t and M. We do this by fitting a power-law relationship to the data obtained from the simulations (Fig. 7), which shows that the slope depends significantly on the environment. As is evident from Fig. 5, none of the models fits the data adequately. Note that there is only a slight difference between isotropic ($\beta = 0$) and anisotropic ($\beta = 0.5$) models. Only if we allow for an unrealistically low value of the slope of the r_{VIR}–M_{VIR} relationship do we get a limited agreement for the DOUBLE cluster, but not for the other two regions.

The slopes of the σ_v–M_0 relationship for different regions and using different group finders seem to be consistent with each other, within the errors (Table 2). None of the theoretical models that we are considering, however, seems to offer a good fit for all the cases. The TIS model seems to give a good fit for the DOUBLE region and for the SKID group finder, but when we use the modified SKID group finder, which produces a sample over a more extended mass interval, we see that the original TIS model does not offer a good fit (Fig. 4).
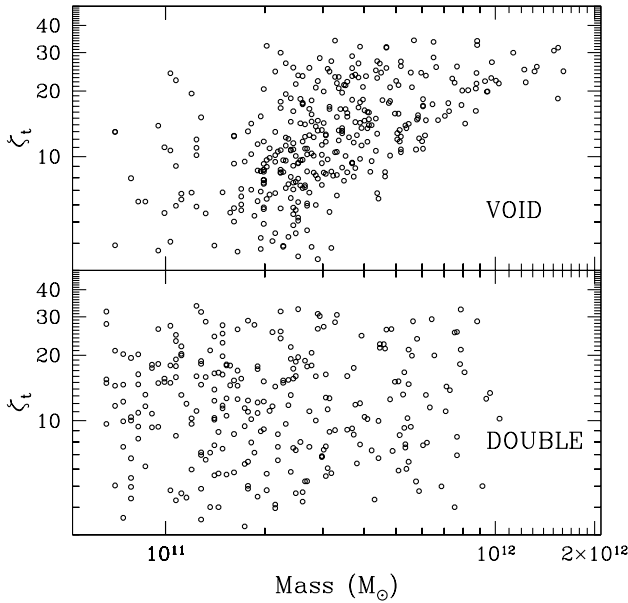
Figure 6. The truncation parameter ζ_t as a function of group mass.
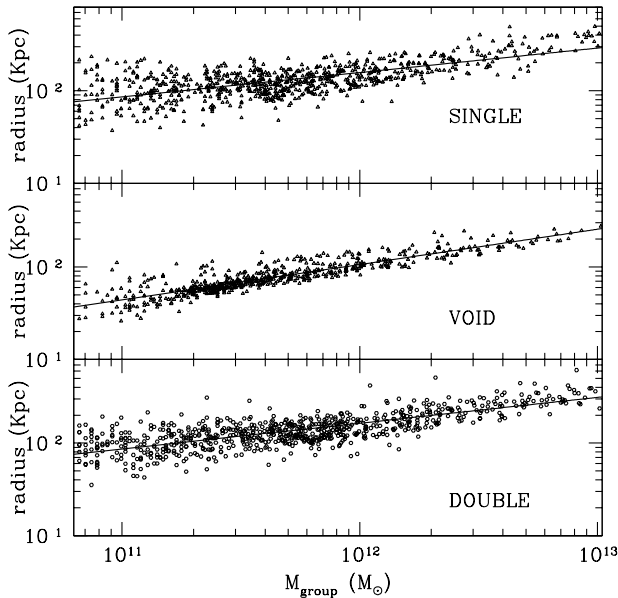

Figure 7. The relationship between truncation radius and mass. Data are fitted using a power-law relationship: $r_t = cM^\alpha$. Least-squares fit values are: $c_{SINGLE} = 1.0789 \times 10^{-1}$, $\alpha_{SINGLE} = 0.2637 \pm 0.1335$; $c_{VOID} = 2.7989 \times 10^{-3}$, $\alpha_{VOID} = 0.3816 \pm 0.0789$; $c_{DOUBLE} = 7.3451 \times 10^{-2}$, $\alpha_{DOUBLE} = 0.2791 \pm 0.1193$.

Note that the rms uncertainty of σ_v in Figs 3–5 is less than $30 \, \mathrm{km \, s^{-1}}$, a value much lower than that found by Knebe & Müller (1999) in their simulations (see their fig. 3). We believe that this is a consequence of the larger mass and force resolution of our simulation, and also of the use of a larger dynamic range than adopted by previous authors.

Generally speaking, a power law seems to offer a good fit for all three regions (although with different ranges for the three regions), but in order to determine the slope one must probably go a step further in modelling the physical state of these haloes. In the next section we will explore in more detail the properties of TIS haloes, and we will focus our attention on their statistical properties.

Table 2. Least-squares best-fitting parameters for σ_v relationship.

Region	α	$\Delta\alpha$	c_0	Method
DOUBLE	0.38	0.08	74.13	SKID
	0.39	0.05	87.74	SKID with HOP input
	0.42	0.07	72.48	AFOF
	0.42	0.03	82.16	TIS selected haloes
SINGLE	0.35	0.04	80.28	SKID
	0.37	0.04	82.15	SKID with HOP input
	0.42	0.07	71.22	Adaptive FOF
VOID	0.39	0.04	86.81	SKID
	0.40	0.04	89.43	SKID with HOP input
	0.45	0.05	63.12	Adaptive FOF
	0.38	0.02	88.60	TIS selected haloes

α, c_0 are the fitting parameters of a power-law fit of the form $\sigma_v = c_0 M_{12}^\alpha$; $\Delta\alpha$ is the rms error associated with α.

4.2 Comparison with the TIS model

We will now consider the possibility of obtaining a reasonable fit of the σ_v–M_0 relationship by modifying the minimum-energy TIS model. We will then present here some more features of this model.

Following Shapiro et al. (1999), the TIS solution is obtained by imposing a finite truncation radius r_t on an isothermal, spherically symmetric collisionless equilibrium configuration. Shapiro et al. define a typical radius:

$$r_0 = \frac{\sigma_v}{(4\pi G\rho_0)^{1/2}}, \tag{9}$$

where ρ_0 is the central density (TIS models are non-singular). Combining the Poisson and the Jeans equilibrium equations, and making the hypothesis of isothermality for the distribution function, they obtain an equation for the dimensionless density (see Shapiro et al. 1999, equation 29):

$$\frac{d}{d\zeta}\left[\zeta^2 \frac{d(\ln\tilde{\rho})}{d\zeta}\right] = -\tilde{\rho}\zeta^2, \tag{10}$$

where we have used the definitions

$$\tilde{\rho} = \frac{\rho}{\rho_0}, \qquad \zeta = \frac{r}{r_0}.$$

Shapiro et al. have shown that non-singular solutions of equation (10) form a one-parameter family depending only on $\zeta_t = r_t/r_0$. The total mass is then given by

$$M_0 = M(r_t) = \int_0^{r_t} 4\pi\rho(r)r^2 \, dr = 4\pi\rho_0 r_0^3 \tilde{M}(\zeta_t), \tag{11}$$

where we have defined a dimensionless total mass:

$$\tilde{M}(\zeta_t) = \frac{1}{r_0}\int_0^{r_t} dr \frac{\rho}{\rho_0}\left(\frac{r}{r_0}\right)^2.$$

We follow further Shapiro et al. (1999, equation 41) and write the virial theorem for a collisionless truncated isothermal sphere:

$$0 = 2K + W + S_p, \tag{12}$$

where $K = M_0 \langle v^2 \rangle / 2 \equiv (3/2) M_0 \sigma_v^2$ and S_p is the surface pressure term. In the Appendix we show that, after some simple algebra,

starting from equation (12) one obtains the following relation:

$$\frac{GM_0}{r_t\sigma_v^2} = \frac{3\tilde{M}(\zeta_t) - \tilde{\rho}(\zeta_t)}{\zeta_t\Psi(\zeta_t)}\tilde{M}(\zeta_t) \equiv \Phi(\zeta_t). \qquad (13)$$

The function $\Psi(\zeta_t)$ is specified in the Appendix.

We have already seen that a power-law fit describes the σ_v–M_0 relationship well. Then from equation (13) we deduce that also the truncation radius r_t has a power-law dependence on the total mass: $r_t \propto c(\zeta_t)M_0^{1-2\alpha}$. Using the values of α from Table 2 we see that the slope of this relationship should lie within the range 0.22–0.3, i.e. it should be quite small. In Fig. 7 we plot r_t as a function of M_0. The best-fitting values that we find for the slope are inconsistent with the predictions from the σ_v–M_0 relationship.

The right-hand side of equation (13) depends only on the dimensionless truncation radius ζ_t, which in the minimum-energy TIS solution of Shapiro et al. (1999) should be fixed to $\zeta_t = 29.4$. The function $\Phi(\zeta_t)$ has a singularity at $\zeta \approx 0.97$, where the denominator goes to zero (Fig. 8). However, we are interested in the region $\zeta_t > 1$, where the truncation radius is at least comparable to the core radius. As is clear from Fig. 8, the function has a minimum at $\zeta \approx 59.5$.

We will look for solutions in the interval $2.91 \leq \zeta_t \leq 59.5$. Within these limits the function $\Phi(\zeta)$ is monotonically decreasing and the solution of equation (13) is certainly unique. Note that the TIS solution is unstable for $\zeta_t > 34.2$ (Antonov 1962; Lynden-Bell & Wood 1968; Shapiro et al. 1999), so our choice of the upper limit will allow us to verify a posteriori this prediction. Equation (13) can be inverted with respect to ζ_t given the left-hand side, because for each group all the quantities on the left-hand side are computed by the group finder. As for the truncation radius r_t we adopt the radius of the groups as computed by SKID, which coincides with the virial radius r_{VIR}.

An interesting feature of the TIS solution, which is evident from Fig. 8, is that in order to invert equation (13) to find ζ_t, the value of the left-hand side must lie within a rather small range of values: $2.75 \leq GM_0/r_t\sigma_v^2 \leq 4.56$. As we can see from Fig. 9 for the case of the DOUBLE region, this is not the case for all the haloes, even for those haloes closely following the σ_v–M_0 relationship. For instance, out of 827 haloes identified by SKID within the DOUBLE region, only 382 lie within the region for which equation (13) can be inverted. For those haloes for which equation (13) can be inverted, we are able to determine ζ_t and to compare it with the predictions of the minimum-energy TIS model. The results of this exercise give us some insight into the properties of these haloes. In Fig. 6 we plot the relationship between ζ_t and the mass for haloes in the VOID and DOUBLE regions (the behaviour of haloes in the SINGLE region is similar to that of those in DOUBLE). The difference between halo properties in these two regions is striking. In the DOUBLE region there is no clear relationship between ζ_t and mass, but we also do not find a clustering around the value $\zeta_t = 29.4$, characterizing the minimum-energy TIS solution as suggested by Shapiro et al. (1999). On the other hand, there seems to be a relationship between ζ_t and mass for haloes in the VOID region, although with a rather large dispersion, particularly for haloes having $M_0 \lesssim 3 \times 10^{11} h^{-1}$ $M_\odot$.

A very interesting property of haloes in Fig. 6 is that we do not find haloes having $\zeta_t \gtrsim 34.2$, the upper limit for gravothermal instability for TIS haloes, although our upper limit for the ζ_t values extends up to $\zeta_t \leq 59.5$. We do, however, also find a few haloes having $\zeta_t < 4.738$, the critical value below which the total energy $E = T + K > 0$ and the TIS solution cannot exist (Shapiro et al.
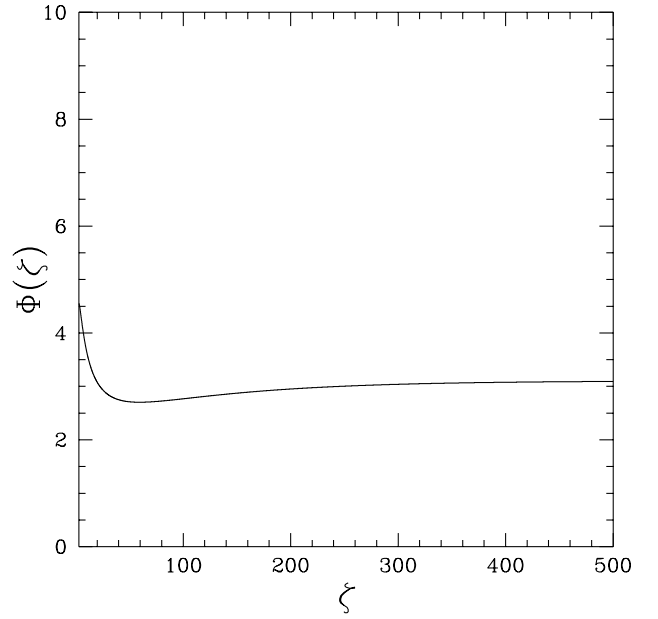

Figure 8. Plot of $\Phi(\zeta_t)$. We start plotting from $\zeta = 0.97$, where the function has an absolute maximum. The vertical scale is the same as that adopted in Fig. 9.
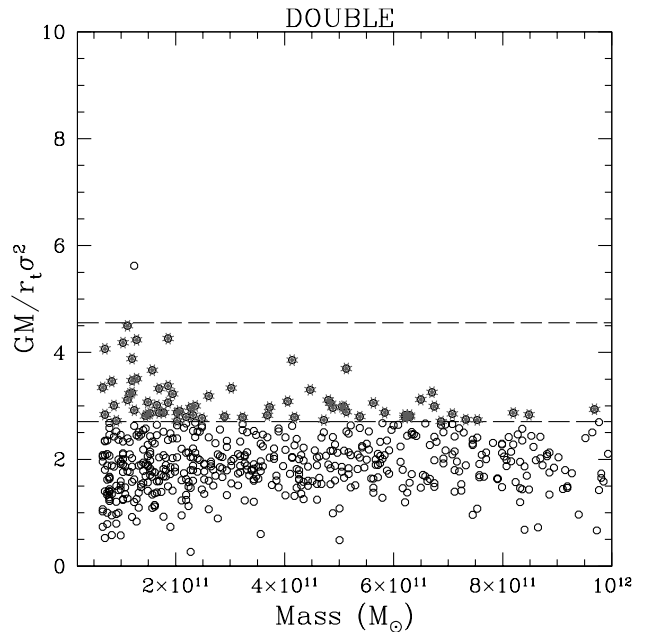
Figure 9. Measured values of $GM_0/r_t\sigma_v^2$ versus mass for the region of the DOUBLE cluster. Groups marked with a star lie within the allowed region where solutions of equation (13) exist, and the corresponding value of ζ_t can be found.

1999). It is important to remember that the haloes we find in a simulation are not spherical and not even 'ideal', being a discrete realization of some equilibrium state, so the above quoted bounds cannot be taken literally.

At first sight, it may seem curious that only a fraction of all the haloes (46 per cent in the DOUBLE and 37 per cent in the VOID, respectively) have values of σ_v and M_0 for which equation (13) can be solved. The obvious interpretation is that only a fraction of haloes have reached equilibrium, even at the end of the simulation;
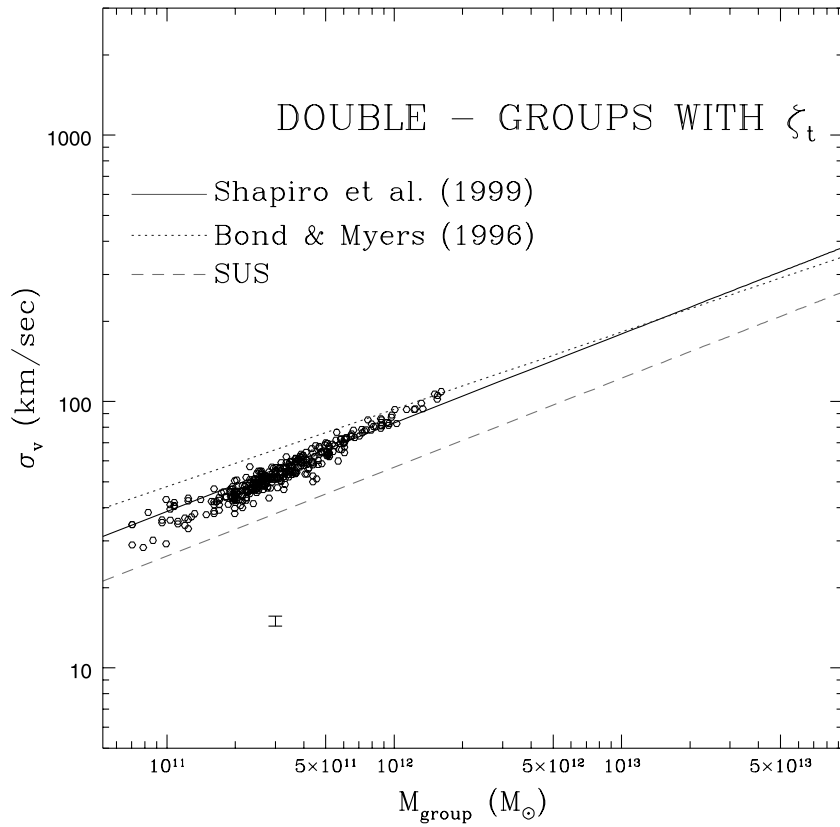
Figure 10. The σ_v–M_0 relation for groups in the DOUBLE region for which the truncation radius can be computed by inverting equation (13). The scatter is less than in the analogous plot for all the groups found by SKID in the DOUBLE region, Fig. 3. The error bar in the lower left part of the plot represents the uncertainty in the zero-point of the best-fitting curve induced by the scatter in observed values of ζ_t. Note that it is less than the observed scatter.

but it also remains a possibility that these 'out-of-equilibrium' haloes relax to an equilibrium state different from any of the three considered in the present work.

Finally, in Figs 10 and 11 we plot the σ_v–M_0 relation of those haloes for which a ζ_t can be found, for the DOUBLE and VOID regions, respectively. Note that for these haloes the intrinsic dispersion is even smaller than in Figs 3 and 4. These haloes can be then regarded as very near to a TIS equilibrium state. Note also that the coefficient of equation (1) for the TIS solution has been computed for the minimum-energy TIS solution. In fact, from equation (98) of Shapiro et al. (1999) we see that this coefficient would depend on ζ:

$$\sigma_v^2 = \frac{(3\pi G)^{2/3}}{5} \frac{\alpha(\zeta)}{\alpha(\zeta) - 2} H_0^{2/3}(1 + z_{\mathrm{coll}})M_0^{2/3}, \qquad (14)$$

where $\alpha(\zeta) = 3\tilde{M}(\zeta)/\zeta^3 \tilde{\rho}(\zeta)$. As we can see from the figures, the scatter induced by this dependence is very small and less than the intrinsic Poisson scatter.

4.3 Probability distribution of the spin parameter

The angular momentum distribution is an interesting statistic, because the halo angular momentum originates from gravitational interactions between the collapsing region and its environment. Following Peebles (1971) and Efstathiou & Jones (1979) we will present results for the distribution of the spin parameter λ defined as

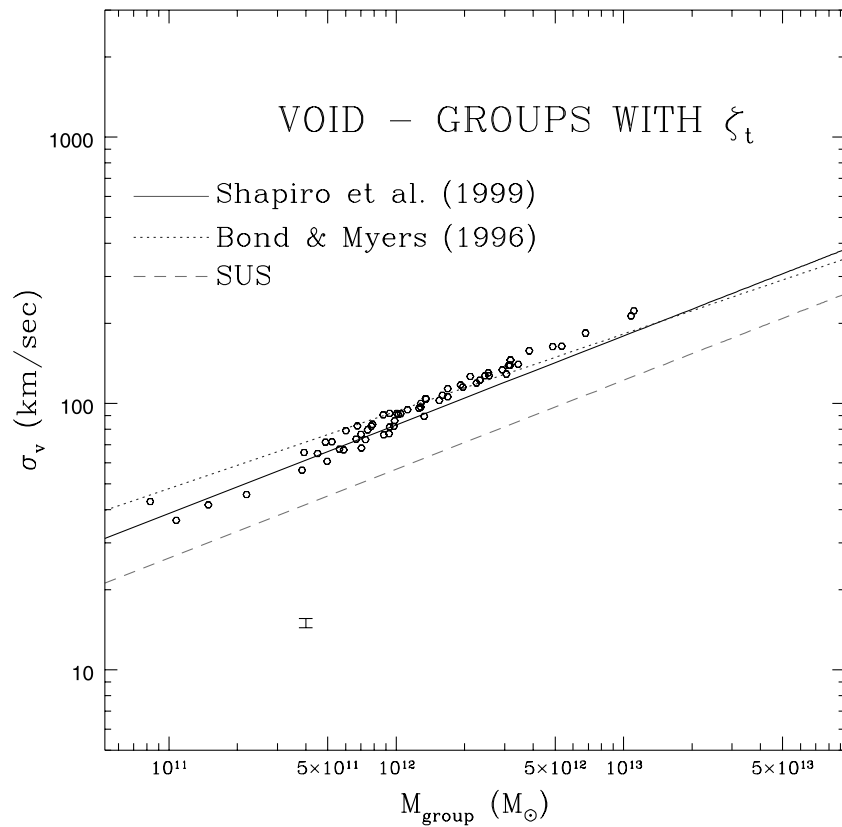$$\lambda = \frac{L|E|^{1/2}}{GM^{5/2}}, \qquad (15)$$

where L and $|E|$ are the angular momentum and the total energy of each halo, respectively. The calculation of $|E|$ is not free of ambiguities, because in order to compute the potential energy W one should take into account the fact that the halo is not isolated, i.e. one should also account for the contribution from the environmental gravitational field, and this is not currently done by any of the group finders we have adopted. For this reason, we show in Fig. 12 the spin probability distribution $P(\lambda)$ computed only for TIS haloes in the three regions, i.e. for those haloes following equation (13). As we have seen in the preceding paragraphs, these haloes seem to follow the σ_v–M_0 relationship with a much smaller scatter than haloes selected by any group finder, so we regard them as our fiducial equilibrium haloes. Combining equations (44) and (45) from Shapiro et al. (1999) we find that for a TIS halo the total energy E is connected to the potential W by

$$E = -\frac{2 - \alpha}{2(\alpha - 1)} W. \qquad (16)$$

The potential W for these haloes is then computed exactly, i.e. by summing the contribution from each particle in the simulation. Note that the parameter α depends on the dimensionless truncation radius ζ_t which can be evaluated only for TIS haloes.

One immediately notices that $P(\lambda)$ seems to depend on the environment. It has been shown in recent work that a very good fit to $P(\lambda)$ is given by a lognormal distribution (Dalcanton, Spergel & Summers 1997; Mo, Mao & White 1998):

$$\lambda P(\lambda) = \frac{1}{\sqrt{2\pi}\sigma_\lambda} \exp\left[-\frac{\ln^2(\lambda/\langle\lambda\rangle)}{2\sigma_\lambda^2}\right] \mathrm{d}\lambda. \qquad (17)$$

Figure 11. As Fig. 10 for the VOID region. Note that the scale of the axes is the same as in Fig. 10.
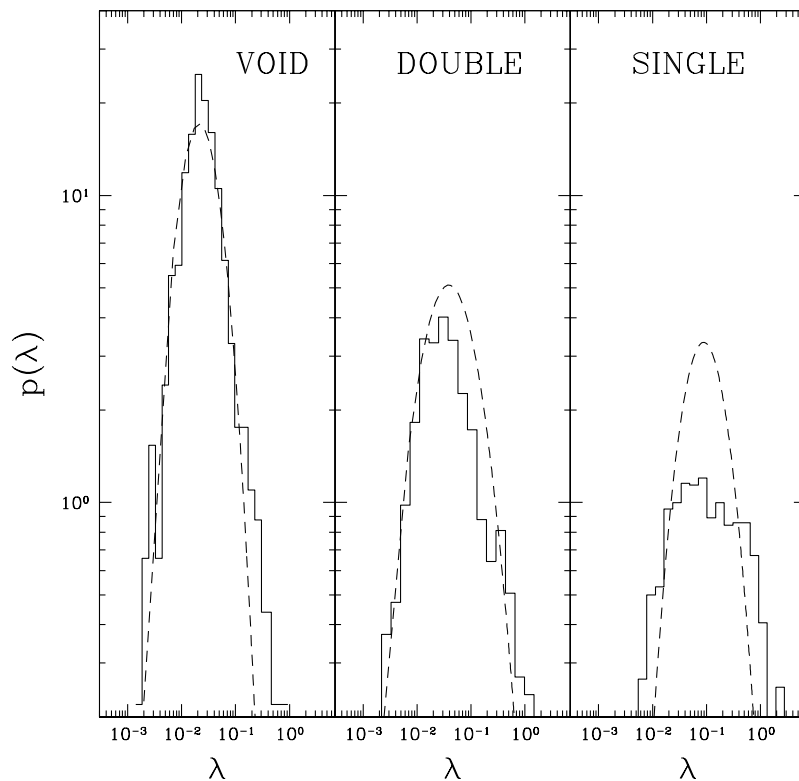
Figure 12. Probability distribution of the spin parameter for the three regions, for TIS haloes. The dashed curves are the best-fitting approximations obtained using the lognormal distribution adopted by (Mo et al. 1998) (equation 15). Histograms and fitting curves are normalized to unity.

Mo et al. (1998) suggest that equation (17) with $\langle\lambda\rangle = 0.05$, $\sigma_\lambda = 0.05$ provides a good fit to the probability distribution of all haloes, independently of the environment. What we observe is, on the other hand, that all three observed distributions seem to be reasonably well fitted by equation (17), but the values of the fitting parameters are certainly very different from those mentioned above. Moreover, for those haloes selected with adaptive FOF, the distributions all seem to be consistent with each other but not well fitted by the lognormal model (Fig. 13). The best-fitting values are presented in Table 3.

This discrepancy may appear puzzling. However, Figs 12 and 13 cannot be compared, for two reasons. First, the total energy E entering the definition of λ was evaluated directly in Fig. 12, while it was estimated from equation (16) in Fig. 13. The procedure that we have adopted to extract *fiducial* TIS haloes does actually produce a sample which follows the $\sigma_v - M_0$ relationship with much less statistical noise than the parent sample. However, there is an even stronger factor that makes the comparison doubtful: the total number of haloes extracted using adaptive FOF is much smaller than that obtained using SKID. Moreover, the extent in λ of the spin probability distribution is smaller than for SKID, as is evident from a comparison of the figures. If we take these differences into account, we do not see any significant difference among the distributions in the VOID region. For all these reasons, we can conclude that there is a dependence of the spin probability distribution $P(\lambda)$ on the environment *only* for TIS haloes. It would be interesting to speculate about the physical mechanisms producing this dependence, and we hope to be able to address this question in further work.
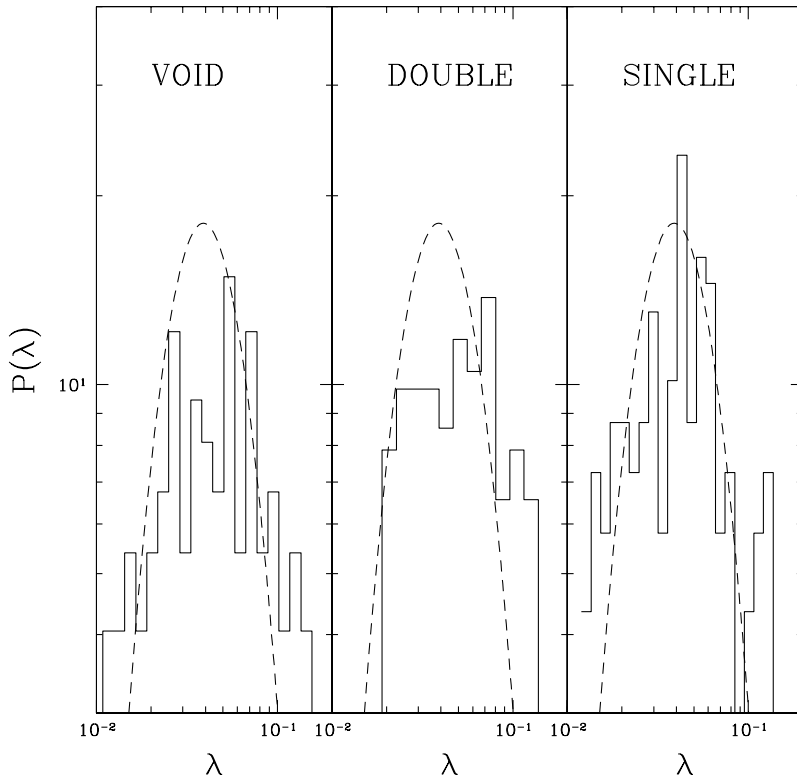
Before closing this section, we would like to remind the reader that recent theoretical calculations predict a rather large distribution in the average values and shape of $P(\lambda)$, with a rather marked dependence on the overdensity of the peak (Catelan & Theuns 1996) or on the details of the merging histories (Nagashima & Gouda 1998; Vitvitska et al. 2001). A direct comparison of our results with the conditional probability distribution $P(\lambda|\nu)$ of Catelan & Theuns (1996) is made difficult by the fact that the relationship between the linear overdensity ν and (for instance) the final mass of the halo turns out to be quite noisy (Sugerman, Summers & Kamionkowski 2000, their fig. 10), so it is not possible to 'label' unambiguously each halo with its initial overdensity. However, one could hope to increase further the number of haloes by further diminishing the softening length, and we hope to get better statistics from future simulations which would help us to address the latter points also.

4.4 Density profiles of massive haloes

As we already mentioned in the Introduction, even the most massive haloes that we find in this simulation using SKID do not contain enough particles to allow a reliable determination of the density profile. This is clearly visible from Fig. 14, where we plot the profiles of the four most massive haloes extracted from the DOUBLE cluster region. None of these haloes lies in the

Table 3. Fits of $P(\lambda)$ with a lognormal distribution, for TIS haloes.

Region	Median	$\langle\lambda\rangle$	σ_λ
VOID	0.018	0.018	0.5
DOUBLE	0.018	0.03	0.9
SINGLE	0.051	0.07	1.4
All (SKID)	0.06	0.07	0.65

Figure 13. As Fig. 12 but for haloes selected using adaptive FOF. The dashed curve is a lognormal distribution with $\langle\lambda\rangle = 0.5$, $\sigma_v = 0.05$.
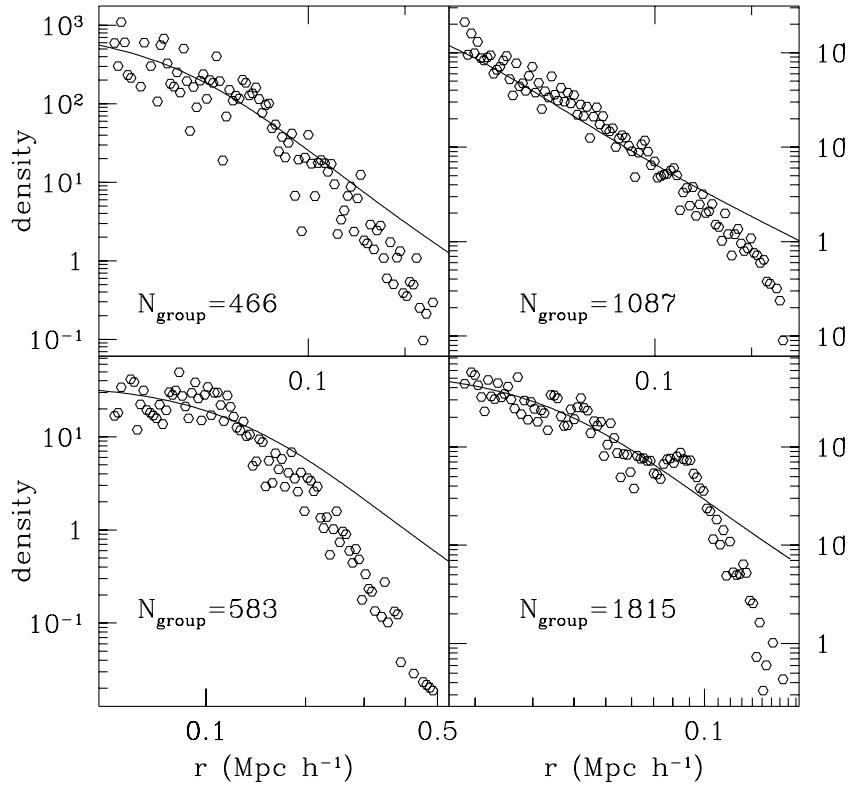
Figure 14. Density profiles for the four most massive haloes within the DOUBLE region. The number of particles contained in each halo is shown. Best-fitting solutions using the minimum-energy TIS solution by Shapiro et al. (1999) are shown.

integrability strip of Fig. 11, so the best-fitting TIS profiles displayed as continuous curves have been obtained by least-squares fittings, where we have varied ρ_0 and r_0.

The distinguishing feature of the TIS density profile, when compared with the universal density profile of Navarro et al. (1996, 1997), is the presence of a central core. Although the minimum-energy TIS profiles fit the central regions reasonably well, they fall off too gently at distances larger than a few times the core radius, and in no case can we find a reasonably good overall agreement. It would be hazardous to draw any conclusion from this comparison, in view of the above-mentioned poor resolution. However, a reasonable explanation for the sharp decline of the density profiles is tidal stripping, which should be effective at a few times the core radius.

5   CONCLUSION

The properties of galaxy-sized haloes that we have considered in this paper seem to be very constraining for halo collapse and equilibrium models. However, none of the equilibrium models considered (or the minimum energy TIS model) seems to be able to give a comprehensive description of our findings. We would now like to summarize our findings and to point to some controversial questions that they pose.

First of all, the σ_v–M_0 statistic seems to be a sensitive tool to discriminate among different halo equilibrium models. This statistic is easy to evaluate, because it relies on global quantities, and it can then be applied to samples of haloes. In this context, it is more difficult to discriminate models using statistics like the density profile, which would require a considerably larger mass

range in order to give reliable results (see for instance Jing & Suto 2000).

Models for the σ_v–M_0 statistic based on the NFW density profile seem to be only marginally consistent with simulation data. The role of the anisotropy parameter in this context does not seem to be crucial: it is the slope of the radius–mass relationship for these haloes that seems mostly to affect the normalization of the σ_v–M_0 statistic.

As we have seen, the TIS model seems to offer a very good quantitative framework to explain the σ_v–M_0 statistic, even in the VOID region where the slope of the relationship is very different from that predicted by the minimum-energy TIS model of Shapiro et al. The fact that a model based on the hypothesis that haloes have a finite extent provides a good description should not come as a surprise. Haloes forming in clusters experience a complex tidal field originating from neighbouring haloes and from the large-scale web in which they are embedded. The tidal radii of the environments within which they lie, although often larger than the mean distance, could limit the extent of haloes. A theoretical treatment of the growth of the angular momentum is complicated by the fact that the distribution of the torques induced by nearby haloes depends on clustering (Antonuccio-Delogu & Atrio-Barandela 1992). However, we believe that it would be difficult to think that the truncation is a numerical artefact resulting from the finite mass resolution: were this the case, we should expect the same relationship between truncation radius r_t and mass in all three regions, but this is clearly not the case.

We have already noted the fact that the truncation radii we find are always less than the critical value for the onset of gravothermal instability, $\zeta_{crit} = 34.2$. This leads us to think that this instability is at work in our simulations, but in order to investigate this issue one

would need simulations with a dynamical range at least 3 orders of magnitude larger than those used in this simulation.

Concerning the dependence of the distribution of spin parameters on the environment, we find that haloes selected using adaptive FOF do not show any dependence on the environment (the same holds for haloes selected using SKID), but if we select subsamples of *fiducial* TIS haloes, we do find a dependence of the properties of $P(\lambda)$ on the environment. In particular, this fact seems to be at odds with the recent investigation by Syer, Mao & Mo (1999), who find that the observed distribution of the spin parameter for a large homogeneous sample of spirals is well described by a lognormal distribution with $\langle\lambda\rangle \approx 0.05$ and a variance $\sigma_\lambda \approx 0.36$. This result is in contrast also with other work (Warren et al. 1992; Eisenstein & Loeb 1995). If confirmed by further investigations, this discrepancy could suggest that there is probably some systematic trend in the way in which the angular momentum of the luminous discs is connected with that of the halo, which is not accounted for by the models of Syer et al. (1999).

Last, but not least, it is important to stress that Lemson & Kauffmann (1999) conclude that 'Only the mass distribution varies as a function of environment. This variation is well described by a simple analytic formula based on the conditional Press–Schechter theory. We find no significant dependence of any other halo property on environment...'. In comparing their results with ours, we must keep in mind that we have followed a very different procedure from theirs, because we have *prepared* a simulation using constrained initial conditions with the purpose of obtaining a final configuration containing certain features (i.e. a double cluster and a void). Although our simulation box is not an 'average' region of the Universe, it is certainly a representative one. We stress again the fact that all the haloes from underdense regions in our simulation come from a void, and not from the outer parts of clusters. Lemson & Kauffmann, on the other hand, seem to take their haloes from all of the volume and group them according to the overdensity of their parent regions. We think then that a direct comparison between the results of these two different investigations would be misleading, given the complementarity of our approaches.

REFERENCES

Antonov V. A., 1962, Solution of the problem of stability of stellar systems with Emden's density law and the spherical distribution of velocities. Vestnik Leningradskogo Universiteta, Leningrad
Antonuccio-Delogu V., Atrio-Barandela F., 1992, ApJ, 392, 403
Barnes J., 1987, Comput. Phys. Commun., 87, 161
Barnes J., Hut P., 1986, Nat, 324, 446
Becciani U., Ansaloni R., Antonuccio-Delogu V., Erbacci G., Gambera M., Pagliaro A., 1997, Comput. Phys. Commun., 106, 105
Becciani U., Antonuccio-Delogu V., Gambera M., Pagliaro A., Ansaloni R., Erbacci G., 1998, in Albrecht R., Hook R. N., Bushouse H. A., eds, ASP Conf. Ser. Vol. 145, Astronomical Data Analysis Software and Systems VII. Astron. Soc. Pac., San Francisco, p. 7
Becciani U., Antonuccio-Delogu V., Gambera M., 2000, J. Comput. Phys., 163, 118

Bertschinger E., 1985, ApJS, 58, 39
Binney J., Tremaine S., 1987, Galactic Dynamics. Princeton Univ. Press, Princeton, NJ
Bond J. R., Myers S. T., 1996a, ApJS, 103, 1
Bond J. R., Mysers S. T., 1996b, ApJS, 103, 41
Bryan G. L., Norman M. L., 1998, ApJ, 495, 80
Buchert T., Kerscher M., Sicka C., 1999, Phys. Rev. D, 62, 043525-1
Bullock J. S., Kolatt T. S., Sigad Y., Somerville R. S., Kravtsov A. V., Klypin A. A., Primack J. R., Dekel A., 2001, MNRAS, 321, 559
Catelan P., Theuns T., 1996, MNRAS, 282, 436
Couchman H. M. P., 1991, ApJ, 368, L23
Dalcanton J. J., Spergel D. N., Summers F. J., 1997, ApJ, 482, 659
Efstathiou G., Jones B. J. T., 1979, MNRAS, 186, 133
Eisenstein D. J., Hut P., 1998, ApJ, 498, 137
Eisenstein D. J., Loeb A., 1995, ApJ, 439, 520
Gardner J., 2000, astro-ph/0006342
Governato F., Moore B., Cen R., Stadel J., Lake G., Quinn T., 1997, New Astron., 2, 91
Gunn J. E., 1977, ApJ, 218, 592
Gunn J. E., Gott J. R. I., 1972, ApJ, 176, 1
Hernquist L., Bouchet F. R., Suto Y., 1991, ApJS, 75, 231
Hoffman Y., Ribak E., 1991, ApJ, 380, L5
Jing Y. P., Suto Y., 2000, ApJ, 529, L69
Knebe A., Müller V., 1999, A&A, 341, 1
Lemson G., Kauffmann G., 1999, MNRAS, 302, 111
Łokas E. L., Mamon G. A., 2001, MNRAS, 321, 155
Lynden-Bell D., Wood R., 1968, MNRAS, 138, 495
Mo H. J., Mao S., White S. D. M., 1998, MNRAS, 295, 319
Moore B., Ghigna S., Governato F., Lake G., Quinn T., Stadel J., Tozzi P., 1999, ApJ, 524, L19
Nagashima M., Gouda N., 1998, MNRAS, 301, 849
Navarro J. F., Frenk C. S., White S. D. M., 1996, ApJ, 462, 563
Navarro J. F., Frenk C. S., White S. D. M., 1997, ApJ, 490, 493
Padmanabhan T., 1993, Structure formation in the universe. Cambridge Univ. Press, Cambridge
Peebles P. J. E., 1971, A&A, 11, 377
Shapiro P. R., Iliev I. T., Raga A. C., 1999, MNRAS, 307, 203
Sugerman B., Summers F. J., Kamionkowski M., 2000, MNRAS, 311, 762
Syer D., Mao S., Mo H. J., 1999, MNRAS, 305, 357
Takada M., Futamase T., 1999, Gen. Relativ. Gravitation, 31, 461
van de Weygaert R., Bertschinger E., 1996, MNRAS, 281, 84
van Kampen E., Katgert P., 1997, MNRAS, 289, 327
Vitvitska M., Klypin M., Kravtsov A., Bullock J., Wechsler R., Primack J., 2001, astro-ph/0105349
Warren M. S., Quinn P. J., Salmon J. K., Zurek W. H., 1992, ApJ, 399, 405
White S. D. M., 1996, in Lahav O., Terlevich E., Terlevich R. J., eds, Proc. 36th Herstmonceux Conf., Gravitational Dynamics. Cambridge Univ. Press, New York, p. 121
White S. D. M., 1997, Dahlem Workshop on the Evolution of the Universe, p. 227
White S. D. M., Rees M. J., 1978, MNRAS, 183, 341

APPENDIX A

We give a full derivation of equation (13). The starting point is the virial theorem for systems with boundary pressure terms, as given in equation (41) from Shapiro et al. (1999):

$$0 = 2K + W + S_p. \tag{A1}$$

In the above equation, the kinetic energy K can be rewritten in terms of the one-dimensional velocity dispersion:

$$K = \frac{M_0\langle v\rangle^2}{2} = \frac{3}{2}M_0\sigma_v^2. \tag{A2}$$

The potential energy term W,

$$W = 4\pi G\int_0^\infty \rho M(r)r\,\mathrm{d}r \equiv 4\pi G\int_0^{r_t} \rho M(r)r\,\mathrm{d}r, \tag{A3}$$

can be rewritten in terms of global quantities and of the dimensionless radius ζ_t:

$$W = -\frac{GM_0^2}{r_t}\frac{\zeta_t\Psi(\zeta_t)}{M^2(\zeta_t)}, \tag{A4}$$

where we have defined

$$\Psi(\zeta_t) = \int_0^{\zeta_t} d\zeta\,\zeta\,\tilde{\rho}(\zeta)\tilde{M}(\zeta).$$

Finally, S_p is a surface term which arises from the constraint that the system has a finite radius, and is given by (Shapiro et al., equation 43)

$$S_p = -4\pi r_0^3 p_t \zeta_t. \tag{A5}$$

We are adopting here the same notation as Shapiro et al., so that r_0 and p_t are the core radius and an external 'pressure' term,

respectively. Using equations (34) and (38) from Shapiro et al., the latter equation can be rewritten in terms of the dimensionless integrated mass and density:

$$S_p = -\frac{M_0}{\tilde{M}_t(\zeta_t)}\tilde{\rho}(\zeta_t)\sigma_v^2. \tag{A6}$$

Substituting equations (A2), (A4) and (A6) into equation (A1), we get

$$3M_0\sigma_v^2 = -\frac{GM_0^2}{r_t}\frac{\zeta_t\Psi(\zeta_t)}{M^2(\zeta_t)} - \frac{M_0}{\tilde{M}_t(\zeta_t)}\tilde{\rho}(\zeta_t)\sigma_v^2, \tag{A7}$$

from which we get the desired equation.